Modeling the Ground and Excited State Unimolecular Decay of the Simplest Fluorinated Criegee Intermediate, HFCOO, formed from the Ozonolysis of Hydrofluoroolefin Refrigerants

Courtney A. Poirier,[1,2] Lily M. Guidry,[1,#] Jordyn M. Ratliff,[1,#] Vincent J. Esposito,[3] Barbara Marchetti[1] and Tolga N. V. Karsili[1,*]

[1]*Department of Chemistry, University of Louisiana at Lafayette, Lafayette, LA 70504, USA*

[2]*Regional Application Center, NASA/University of Louisiana at Lafayette, Lafayette, LA 70506, USA*

[3]*Vincent J. Esposito, NASA Postdoctoral Program Fellow, NASA Ames Research Center, Moffett Field, CA 94035-1000*

*author to whom correspondence should be addressed, tolga.karsili@louisiana.edu

[#]authors contributed as undergraduate research students.

Abstract

Hydrofluoroolefins (HFO) are fourth generation refrigerants designed to function as efficient refrigerants with no ozone depletion potential and zero global warming potential. Despite extensive studies on their chemical and physical properties, the ground and excited state chemistry of their atmospheric oxidation products is less well understood. This study focuses on the ground and excited state chemistry of the simplest fluorinated Criegee intermediate, fluroformaldehyde oxide (HFCOO), which is the simplest fluorinate Criegee intermediate formed from the ozonolysis of HFOs. HFCOO contains *syn* and *anti* conformers, which have Boltzmann populations of, respectively, 87 % and 13 % at 298 K. For both conformers, the calculated ground state reaction energy profiles associated with cyclization to form fluror-dioxirane is lower than the equivalent unimolecular decay path in the simplest Criegee intermediate, H_2COO; with *anti*-HFCOO returning a barrier height more than half that of H_2COO. The excited state dynamics reveal that photoexcitation to the bright S_2 state of *syn*-HFCOO and *anti*-HFCOO is expected to undergo prompt O-O fission – with the former conformer expected to dissociate with an almost unity quantum yield and to form both O (^{1}D) + HFCO (S_0) and O (^{3}P) + HFCO (T_1) products. In contrast, photoexcitation of *anti*-HFCOO is expected to undergo O-O bond fission with a non-unity quantum yield. The fraction of photoexcited *anti*-HFCOO that dissociates is predicted to exclusively form O (^{1}D) + HFCO (S_0) products, which is in sharp contrast to H_2COO. The wider implications of our results are discussed from both physical and atmospheric chemistry perpectives.

1. Introduction

Hydrofluoroolefins (HFOs) are a class of molecules that find use in modern day refrigerants.[1–3] They are fourth generation refrigerants manufactured to replace chlorofluorocarbons (CFCs), hydrochlorofluorocarbons (HCFCs), and hydrofluorocarbons (HFCs). In contrast to CFCs, HCFCs, and HFCs, refrigerants containing HFOs and HFO blends contain no ozone depletion potential and very low global warming potential.[4,5] These latter characteristics are mostly due to their short lifetimes in the troposphere, undergoing oxidation via tropospheric OH radicals and O_3.[6,7]

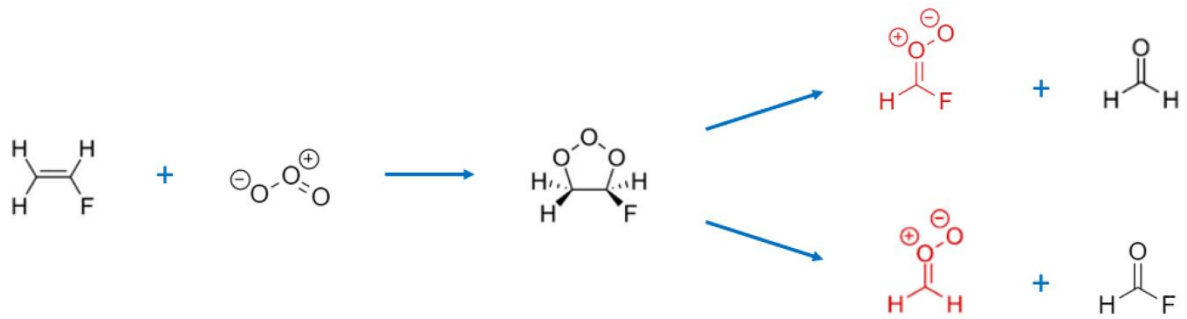

Figure 1: Schematic reaction path showing the ozonolysis of the simplest HFO. The molecules of interest in this study is shown in red.

Despite the plethora of research on HFO molecules, very little is known about the fate of their oxidation products once they are broken down in the atmosphere. Their nascent products may have non-negligible effects in the troposphere, while the π-perturbing effects of the F-substituent may enable these fluorinated oxidation products to display some interesting (photo)chemistry, which may appeal to the wider physical and organic chemistry community. Fluorine is a unique substituent as it contains both σ- and π- perturbing characteristics. It induces a mild σ-withdrawing effect and a strong π-donating effect. Together these two effects are able to perturb the electron-density distribution in molecular systems and induce interesting chemistry. In this

article, we focus on the reaction of HFOs with ozone – which is expected to proceed via ozonolysis across the olefinic C=C bond. Fig. 1 illustrates the expected ozonolysis reaction of the simplest HFO. As shown, ozonolysis proceeds via a [3+2]-cycloaddition of ozone across the C=C double bond of the HFO – forming a primary ozonide (POZ). By analogy with related systems, the POZ is expected to be formed highly internally excited and undergo unimolecular decay to form HFCO and HFCOO products. The latter is known as the Criegee intermediate (CI), which has been the center of a numerous studies due to its atmospheric relevance.[8–11]

Non-fluorine containing CIs are formed in the atmosphere when olefinic volatile organic compounds are emitted into the troposphere via human activity or terrestrial vegetation.[12,13] The simplest CI, formaldehyde oxide (H_2COO), is formed highly internally excited via an analogous ozonolysis process describe above. The highly internally excited H_2COO may also undergo unimolecular decay or collide with proximal vapor molecules and collisionally relax to form stabilized H_2COO. The stabilized H_2COO may also undergo unimolecular decay or bimolecular chemistry with proximal vapor molecules. Unimolecular decay of H_2COO is dominated by cyclization to form dioxirane, which also undergoes unimolecular decay to form bisoxy biradical products.[14–16] This latter biradical undergoes isomerization to form CO_2 + H_2, CO + H_2O or internally excited formic acid, which decays to form OH + HCO radical products. In the troposphere, this unimolecular decay competes with bimolecular chemistry with trace gases such as water, SO_2, NO_x, alcohols and organic acids.[17,18,27,19–26] Reaction with water dominates the bimolecular chemistry of H_2COO (and is its major sink) reacting with either water monomer or dimer to form hydroxymethyl-hydroperoxide. Photochemical studies on H_2COO have also attracted some attention.[19,24,35–37,25,28–34] Lester and co-workers have undertaken electronic absorption spectroscopy and velocity map imaging studies on jet-cooled H_2COO molecules,

showing photodissociation to form H_2CO + O products following excitation at $\lambda < 340$ nm.[32] At elevated UV photon energies, both O (^1D) and O (^3P) products are detected, which are accompanied by the H_2CO (S_0) and H_2CO (T_1) counter-fragments, respectively. High-level electronic structure calculations reveal that the S_2 state carries the high absorption cross section, and O-O bond dissociation leads to two spin-allowed singlet asymptotes. The O (^1D) + H_2CO (S_0) and O (^3P) + H_2CO (T_1) products represent the first and second dissociation asymptotes, respectively. Using "on-the-fly" trajectory surface hopping, with energies, gradients and non-adiabatic couplings calculated using MS-CASPT2, our group recently showed that vertical electronic excitation to the S_2 state leads to prompt O-O bond dissociation and a 80:20 branching ratio in favor of the lower O (^1D) + H_2CO (S_0) asymptote.[35] The formation of O(^1D) may have profound implications in the atmosphere since its reaction with water in humid conditions leads to the formation of OH radicals that enhance the oxidizing capacity of the troposphere.

In this manuscript we compare and contrast the ground and excited state unimolecular decay of H_2COO and HFCOO, in order to ascertain the effect of fluorination to the ground state unimolecular decay kinetics and the photodissociation dynamics.

2. Methodology

Using the Molpro computational package, the ground state minimum energy geometries of H_2COO and HFCOO, as well as their respective dioxirane products and associated transition states, were optimized at the DF-CCSD(T)-F12/aug-cc-pVTZ level of theory. Associated normal mode wavenumbers were also computed on the optimized structures at the same level of theory. Single point energy calculations were then carried out at the CCSD(T)-F12/cc-pVQZ-F12 level of theory in order to obtain more accurate energies on the optimized structures.

Following our prior work on H_2COO, the fate of the excited states of HFCOO was modelled in two ways: direct dynamics via full-dimensional trajectory surface hopping and static electronic structure calculations to explore the topologies of the key excited state reaction paths. Trajectory surface hopping (TSH) simulations were performed using the Newton-X computational package.[38,39] To remain consistent with our prior work, initial conditions were obtained by means of a Wigner distribution based on the B2PLYP-D3/cc-pVTZ equilibrium geometry of the HFCOO and the associated harmonic normal mode wavenumbers. This level of theory (executed in Gaussian 16) has been shown to perform well in determining geometries and normal modes of CIs and their reactions.[31,32,35–37,40–42] Since our prior trajectory simulations on H_2COO were based on a Wigner distribution that were also based on an optimized geometry/normal modes from this level of DFT, we use this here for a consistent comparison. We[31,33] and others[43–49] have shown that a Wigner distribution has been successful in predicting the electronic absorption spectra of atmospherically relevant molecules, including Criegee intermediates, and that the choice of DFT functional has a negligible effect on the simulated electronic absorption spectrum – especially when the absorption spectrum is computed using a higher level multi-reference method. In TSH, the nuclei are propagated by integrating Newton's equation using the velocity Verlet method, while the electronic coordinates were propagated by numerically solving the time-dependent Schrödinger equation using Butcher's fifth-order Runge-Kutta method in steps of 0.025 fs.[50] Trajectories were initiated in the S_2 state and the energies and gradients of the seven lowest singlet states were calculated "on-the-fly" using the single-state, single-reference multistate complete active space second order perturbation theory (SS-SR-CASPT2) method in conjunction with the cc-pVDZ basis set.[51] SS-SR-CASPT2 enables the computation of energies and analytical gradients at MS-CASPT2 quality, at a reduced computational cost; it also

performs well near electronic state degeneracies. The SS-SR-CASPT2 calculations were based on a state-averaged complete active space self-consistent field (CASSCF) method reference wavefunction and an active space comprising 10 electrons in 8 orbitals as depicted in Fig. S1 of the supporting information. These were performed via the BAGEL interface to Newton-X.[52] The state hopping probabilities were evaluated by calculating the non-adiabatic coupling matrix elements from the SS-SR-CASPT2 computations.

Using Molpro, additional excited state reaction paths were constructed along the O-O stretch coordinate using the CASPT2/aug-cc-pVTZ level of theory. The same 10/8 active space as the above TSH simulations was used for these computations.

3. Results and Discussion

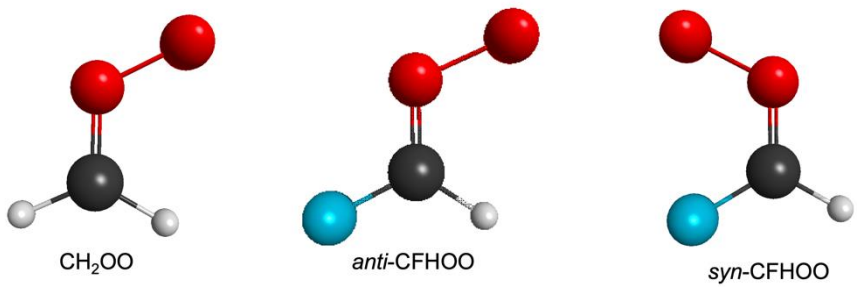

Figure 2: ground state minimum energy geometries of H_2COO, *anti*-HFCOO and *syn*-HFCOO optimized at the DF-CCSD(T)-F12/aug-cc-pVTZ level of theory.

Fig. 2 presents the ground state minimum energy geometry of the lowest two conformers of HFCOO, alongside the minimum energy geometry of H_2COO. These conformers are distinguishable by whether the terminal oxygen atom is pointing towards (*syn*-) or away (*anti*-) from the fluorine atom. In all cases, all atoms are in a common plane with the CO and OO bond distances of ca. 1.24 Å and 1.38 Å, respectively, for *syn*-/*anti*-HFCOO. When compared to H_2COO, the CO (1.27 Å) and OO (1.34 Å) bond distances of HFCOO are comparable, with only

mild changes in the distances due to the fluorine substituent. The slight elongation of the OO bond and slight shortening of the CO bond might indicate greater Zwitterionic character in HFCOO (cf. H_2COO). The *syn*- conformer is ca. 1 kcal mol^{-1} more stable than the *anti*-conformer, manifesting in calculated Boltzmann populations of 87 % (anti) and 13% (syn) at 298 K.

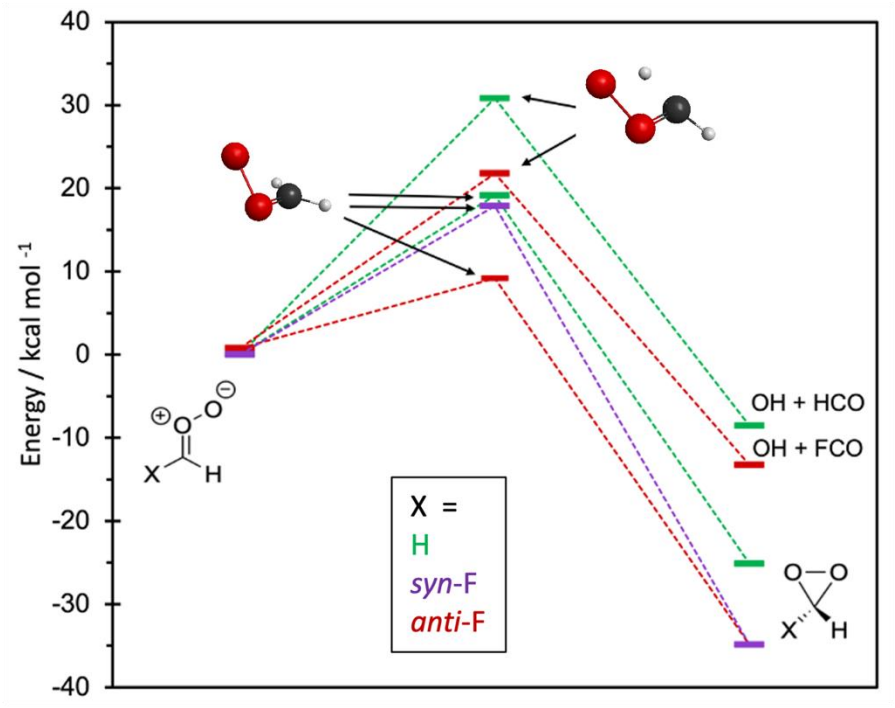

Figure 3: Zero point corrected CCSD(T)-F12/cc-pVQZ-F12//DF-CCDS(T)-F12/aug-cc-pVTZ energies associated with dioxirane formation of H_2COO, *syn*-HFCOO and *anti*-HFCOO.

We now turn our attention to the unimolecular decay paths available to thermalized and electronically excited HFCOO and compare these unimolecular decay paths to the simplest CI, H_2COO. By analogy with H_2COO, the dominant unimolecular decay path available to HFCOO is expected to be via cyclization to form dioxirane. Fig. 3 presents the reaction energy profiles associated with the minimum energy paths connecting the parent HFCOO and H_2COO structures to their dioxirane products. All energies are relative the lowest energy conformer of the parent

CI. The returned CCSD(T)-F12/cc-pVQZ-F12//DF-CCDS(T)-F12/aug-cc-pVTZ barrier height for H_2COO is ca. 20 kcal mol^{-1} while the reaction energy change for forming dioxirane from H_2COO is -26.3 kcal mol^{-1}. Both values are in excellent agreement with previously reported high-fidelity electronic structure calculations of this same reaction path,[16] which reassures us that this level of theory is sufficient in providing highly accurate reaction energy profiles for HFCOO. Using the same level of theory, HFCOO is expected to undergo cyclization to form the fluoro-dioxirane products with an exothermicity which is ca. 10 kcal mol^{-1} greater than cyclization of H_2COO.

This may be a consequence of the stability of fluoro-dioxirane (cf. bare dioxirane), which can be understood by recognizing the higher bond order of the C-F bond associated with the greater electrostatic attraction between C and F. This is in good agreement with calculated heats of formation of difluorodioxirane, which suggest that the F substituents stabilized the dioxirane (cf. bare dioxirane) to a greater extent than the parent F_2COO (cf. H_2COO).[53] Additionally, the transition state barrier associated with the cyclization of HFCOO is lower than the equivalent cyclization of H_2COO. This effect is more dramatic in *anti*-HFCOO, which shows a transition state barrier that is ca. 10 kcal mol^{-1} lower than the equivalent transition state barrier in H_2COO. The lowering of the transition state barrier is plausibly explained by recognizing the mild π-perturbing characteristics of fluorine (cf. hydrogen). As fluorine is a π-donor, it seeks to increase electron-density centered across the COO π-system, introducing additional electron repulsion. The latter effect is expected to weaken the π-system, thus enabling facile motion out-of-plane. When comparing *syn*-HFCOO with *anti*-HFCOO, the former transition state for cyclization is ca. 8 kcal mol^{-1} higher. This higher barrier likely arises via the greater stability of the parent *syn*-HFCOO molecule via halogen bonding, as the *p*π lone-pair on F interacts with the π*-orbital

localized around the COO moiety. Motion out-of-plane is thus expected to break this favorable interaction. We therefore expect that unimolecular decay via cyclization is likely to occur at a faster rate for HFCOO (cf. H_2COO). Figure 3 also compares the 1,3-hydrogen migration paths for H_2COO and *anti*-HFCOO to form OH + XCO (where X = H or F) products. While the barrier associated with this path is ca. 30 kcal mol^{-1} in H_2COO, that for *anti*-HFCOO is less than 20 kcal mol^{-1} and at the same energetic threshold as the 1,4-hydrogen migration that dominates the unimolecular decay of alkyl substituted CIs.

Next, we compare the excited state dynamics of *syn*-/*anti*-HFCOO with H_2COO. Table 1 lists the vertical excitation energies and oscillator strengths associated with excitation to the lowest two excited states of H_2COO, *syn*- HFCOO and *anti*-HFCOO.

Table 1: Vertical excitation energies, in eV (nm), and oscillator strengths associated with excitation to the S_1 and S_2 states of H_2COO, *syn*-HFCOO, and *anti*-HFCOO.

Transition	**H_2COO**		***Syn*-HFCOO**		***Anti*-HFCOO**	
	Vertical Excitation Energy	**Oscillator Strength**	**Vertical Excitation Energy**	**Oscillator Strength**	**Vertical Excitation Energy**	**Oscillator Strength**
$S_1 \leftarrow S_0$	2.34 eV (526.8 nm)	0.000	2.83 eV (437.2 nm)	0.000	2.75 eV (451.5 nm)	0.000
$S_2 \leftarrow S_0$	3.73 eV (332.2 nm)	0.094	3.82 eV (324.8 nm)	0.092	3.21 eV (385.7 nm)	0.064

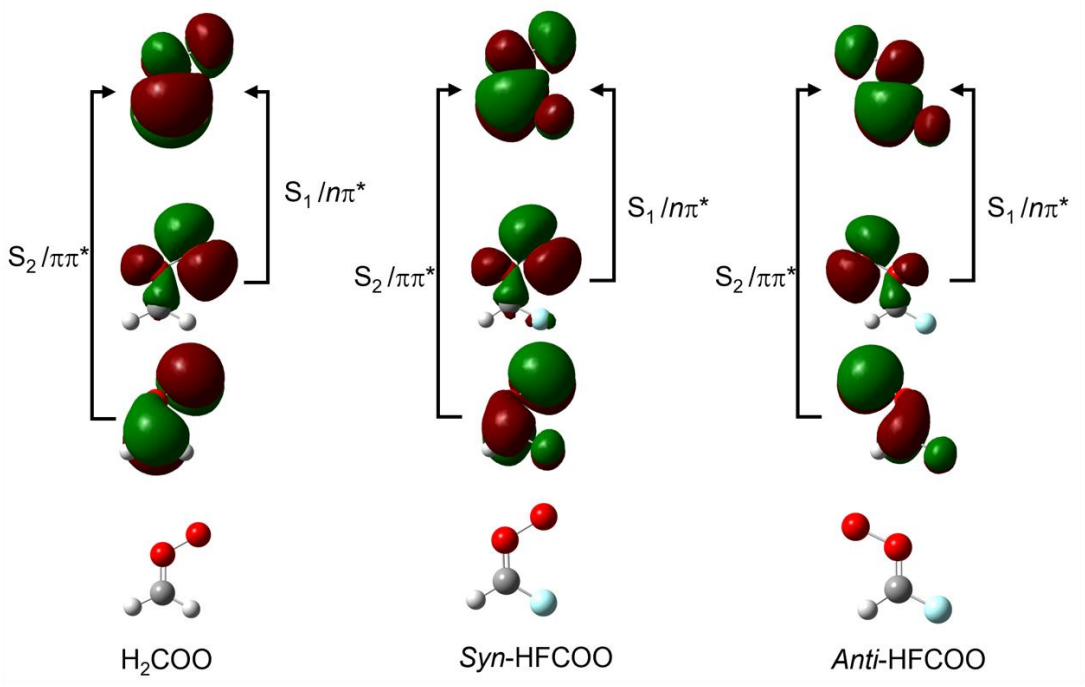

Figure 4: Orbitals and dominant orbital promotions associated with excitation to the S_1 and S_2 states of H_2COO, *syn*-HFCOO, and *anti*-HFCOO.

As Table 1 shows, the S_1 state in all three cases is dark – arising via an electron promotion from an n to a π* orbital, as shown in Fig. 4. The zero-oscillator strength can be understood by recognizing the poor spatial overlap between the participating n and π* orbitals. In contrast, the S_2 state contains a high oscillator strength and, as shown in Fig. 4, arises via a π to π* electron promotion. The high oscillator strength is a manifestation of the high spatial overlap between the participating orbitals involved in the electronic excitation.

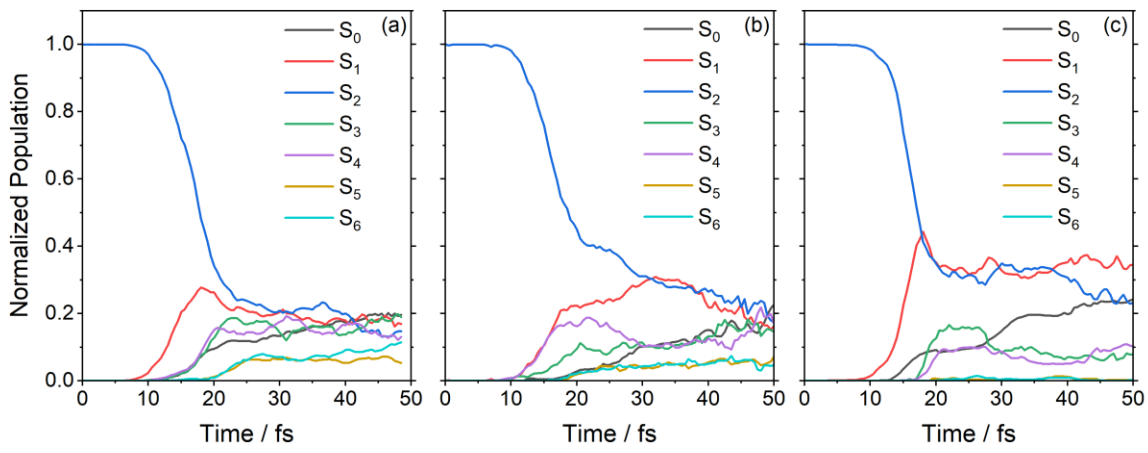

Figure 5: Population as a function of time following excitation to the S_2 state of (a) H_2COO, (b) *syn*-HFCOO, and (c) *anti*-HFCOO. The data for (a) is taken from ref. [37].

In order to study the dynamics following excitation to the S_2 state, TSH simulations were undertaken. Fig. 5 and 6 displays the returned population and the O-O bond lengths as a function of time of (a) H_2COO, (b) *syn*-HFCOO, and (c) *anti*-HFCOO, respectively. Figure 7 illustrates the calculated PE curves as a function of the O-O stretch for (a) H_2COO, (b) *syn*-HFCOO, and (c) *anti*-HFCOO. The PE profiles (Fig. 7) are now well-known for CIs, so only a brief account will be given here. In all cases, the S_1, S_2, S_3 and S_4 states adiabatically correlate with the lower energy singlet asymptote corresponding to O (^{1}D) + aldehyde (S_0) products, while the S_5 and S_6 states adiabatically correlate with the O (^{3}P) + aldehyde (T_1) products.

The TSH data displayed in Fig. 5(a) is from our prior work,[37] which shows the pre-excited S_2 state depopulate within ca. 20 fs and with all trajectories undergoing O-O bond fission within 50 fs. This latter statement is clearly illustrated in Fig. 6(a) that show that all trajectories undergo O-O bond elongation within 50 fs. At 50 fs, the S_0-S_4 states, which correlate with O (^{1}D) + H_2CO (S_0) products, carry 80 % of the population, while the S_5 and S_6 states carry the remaining 20 % of the population. These latter states correlate with the O (^{3}P) + H_2CO (T_1) products. Similarly,

the TSH simulations for *syn*-HFCOO show that the majority of the trajectories undergo O-O bond fission in 50 fs, with a small fraction of trajectories (ca. 5%) remaining at R_{OO} < 2.4 Å at 50 fs (Fig. 6(b)). In contrast, a smaller fraction of trajectories dissociate on the S_5 and S_6 states (ca. 10%) to form O (^{3}P) + HFCO (T_1) products. This latter observation is more significant in *anti*-HFCOO (Fig. 5(c)) wherein no fraction of the preexcitated population partitions to the S_5 and S_6 states – implying no O (^{3}P) + HFCO (T_1) products.

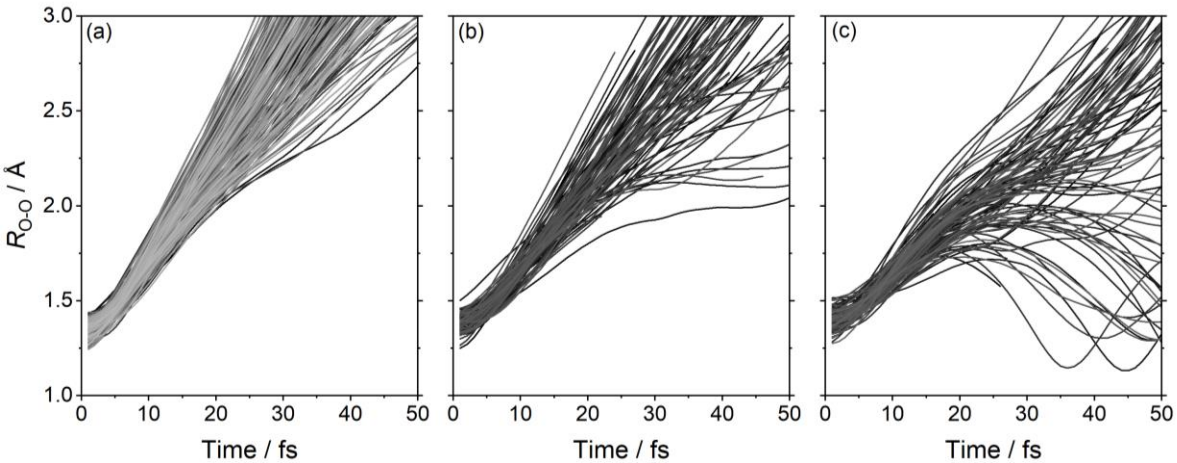

Figure 6: The O-O bond distance of each trajectory as a function of time for (a) H_2COO, (b) *syn*-HFCOO, and (c) *anti*-HFCOO. The data for (a) is taken from ref. [37].

The far lower yield of O (^{3}P) + HFCO (T_1) products for photoexcited HFCOO can be understood by comparing the calculated CASPT2 PE profiles along the O-O bond stretch coordinate of H_2COO and HFCOO (Fig. 7). In the case of H_2COO (Fig. 7(a)), vertical excitation at ca. 3.7 eV is above the energetic threshold for forming both the O (^{1}D) + H_2CO (S_0) and O (^{3}P) + H_2CO (T_1) asymptote limits. In contrast, the vertical region of the S_2 state of HFCOO (Figs. 7(b) and 7(c)) is below the energetic threshold for forming the O (^{3}P) + H_2CO (T_1) products. This effect is more dramatic in *anti*-HFCOO which shows a significant bathochromic shift in the vertical excitation energy (see Fig. 7 and Table 1) when compared to H_2COO and HFCOO – which is

significantly below the energetic limit for forming O (^{3}P) + H_2CO (T_1) products. Since the PE profiles in Fig. 7 are unrelaxed, local distortions and structural relaxations are expected to lower the energetic threshold of the O (^{3}P) + H_2CO (T_1) asymptote limits, which plausibly explains the observation of population in the S_5 and S_6 states in *syn*-HFCOO at 50 fs (Fig. 5(b)). This is supported by analysing the trajectories that partition to the S_5 and S_6 states, which correlate with the HFCO(T_1) + O(^{3}P) products. Fig. 8 displays example trajectories that partition to the S_5 and S_6 states. In both case the HFCO geometry undergoes pyramalization upon O-O bond elongation which is analogous to our previous observations in H_2COO.[54] The pyramindalization can be understood by recognizing that the minimum energy geometry of formaldehyde (H_2CO) is pyramidal in its T_1. Such local relaxation will lower the energetic threshold for forming O(^{3}P) + HFCO (T_1) products and enable population of this product limit upon vertical excitation to the S_2 state.

In contrast, such structural relaxations are unlikely to lower the O (^{3}P) + H_2CO (T_1) asymptote limit to energies that are comparable to the S_2 vertical excitation energy of *anti*-HFCOO. This latter statement plausibly explains the lack of population in the S_5 and S_6 states of *anti*-HFCOO in Fig. 5(c). Since the S_2 state in *anti*-HFCOO supports a deeper potential energy well (cf. *syn*-HFCOO), this is expected to contribute to a greater fraction of population trapped in the vertical region. This is also reflected in the oscillations observed for a number of trajectories in Fig. 6 (c), which indicates multiple vibrational periods of O-O stretch, showing that within the 50 fs time-window, these trajectories remain as parent *anti*-HFCOO molecules. This observation aligns with our previous studies on methyl vinyl ketone oxide and methacrolein oxide.[36]

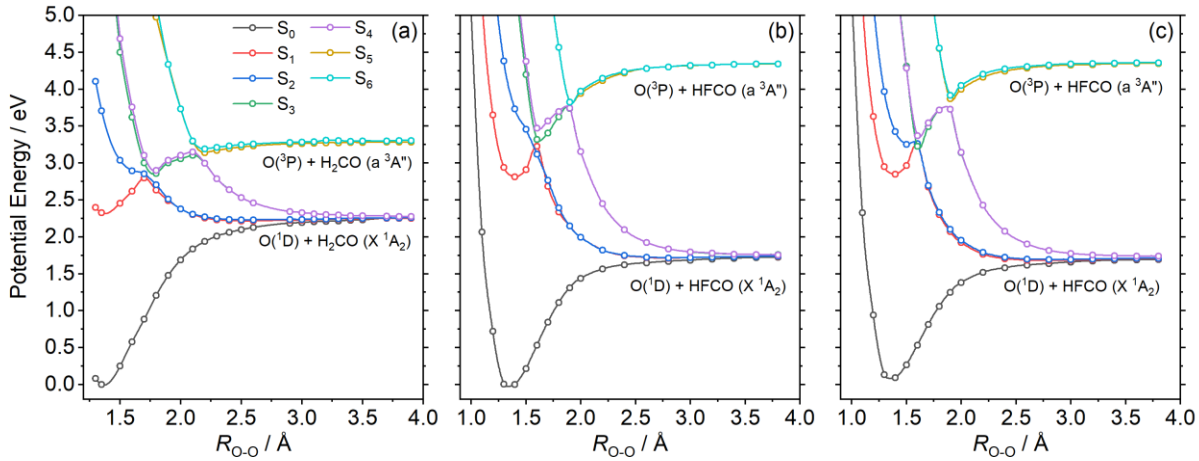

Figure 7: CASPT2 Potential energy profiles of (a) H_2COO, (b) *syn*-HFCOO, and (c) *anti*-HFCOO, computed along the O-O bond stretch coordinate (R_{OO}). The data for (a) is taken from ref. [32].

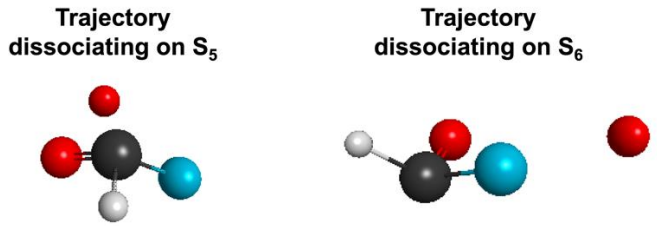

Figure 8: Configurations of example trajectories dissociating on the S_5 and S_6 states.

4. Conclusions

In this article we have undertaken high-level electronic structure and dynamics simulations to study the ground and excited state unimolecular chemistry of the simplest fluorinated CI, HFCOO. Unlike H_2COO, the simplest CI, HFCOO contains *syn* and *anti* conformers with

calculated conformer populations of 87% and 13% in *syn* and *anti*, respectively. Guided by H_2COO, we explored the ground state cyclization of HFCOO to form dioxirane and OH + FCO products. In both unimolecular decay types, the transition state barrier associated with cyclization substantially lower for HFCOO (cf. H_2COO). This observation may be relevant to atmospheric chemistry but may also have broader implications for the physical and synthetic chemistry community.

Guided by the equivalent reaction path in H_2COO, we conclude that the nascent fluoro-dioxirane will undergo unimolecular decay to form FCOOH, FCO + OH radicals, CO_2 + HF, or CO + HOF (hypofluorous acid). Predicted energies for these decay products are reported in table S2, which are all below the energetic barrier for cyclization. Since we have not performed a detailed reaction energy profile analysis leading to the products, we can only infer the viability of these products from the resulting dioxirane. Since, these products may have significant global warming potential and impact various atmospheric processes such as acid rain formation, and thus should be considered in future studies, and in future atmospheric models.

Additionally, we have also explored the excited state dynamics of *syn*- and *anti*- HFCOO. While *syn*-HFCOO undergoes electronic absorption on the short wavelength edge of the tropospherically relevant solar irradiance, *anti*-HFCOO absorbs at a region of the solar irradiance which is ca. 3 times actinic flux (cf. *syn*-HFCOO). As such, *anti*-HFCOO may undergo solar light induced O-O bond fission to form HFCO + O (^{1}D) products. The excited state dynamics of HFCOO *versus* H_2COO is also interesting from a physical chemistry perspective. Our previous studies on the excited state dynamics of H_2COO revealed that following excitation to the S_2 state, O-O bond fission within 50 fs leads to O (^{1}D) + H_2CO (S_0) and O (^{3}P) + H_2CO (T_1) products with an 80:20 branching ratio. The equivalent excitation of *syn*-HFCOO reveals a 10 %

reduction in O (^{3}P) + HFCO products, while this latter channel is completely quenched in electronically excited *anti*-HFCOO. To the best of our knowledge, this is the first illustration that the branching into the O (^{3}P) products is completely quenched. This observation may have atmospheric implications since it promotes the formation of O(^{1}D) products that are known to promptly react with water to form OH radicals. Such observations may also be relevant for the wider photochemistry community as it shows how branching fractions at conical intersection are perturbed by remote substitution.

Overall, this study reveals that although HFO contain no global warming potential, the ground and excited state chemistry of its ozonolysis products may undergo unimolecular decay to form products with non-negligible global warming potential. Our future studies will focus on the bimolecular chemistry of HFCOO as well as the ground and excited state unimolecular decay and bimolecular chemistry of the second CI formed during the ozonolysis of HFO-1234ze – CF_3CHOO (displayed in Fig. 1).

Acknowledgments

The work reported in this article is supported by the National Science Foundation, under grant no. 2003422. C.A.P thanks the National Science Foundation (2120015) for the award of a research assistantship. V.J.E's research was supported by an appointment to the NASA Postdoctoral Program at the NASA Ames Research Center, administered by Oak Ridge Associated Universities under contract with NASA. Portions of this research were conducted with high performance computational resources provided by the Louisiana Optical Network Infrastructure (http://www.loni.org).

Supporting Information

Active space orbitals for the CASSCF/CASPT2 calculations.

The authors declare no conflicts of interest

References

(1) Mateu-Royo, C.; Navarro-Esbrí, J.; Mota-Babiloni, A.; Amat-Albuixech, M.; Molés, F. Thermodynamic Analysis of Low GWP Alternatives to HFC-245fa in High-Temperature Heat Pumps: HCFO-1224yd(Z), HCFO-1233zd(E) and HFO-1336mzz(Z). *Appl. Therm. Eng.* **2019**, *152*, 762–777. https://doi.org/https://doi.org/10.1016/j.applthermaleng.2019.02.047.

(2) Molés, F.; Navarro-Esbrí, J.; Peris, B.; Mota-Babiloni, A.; Barragán-Cervera, Á.; Kontomaris, K. (Kostas). Thermo-Economic Evaluation of Low Global Warming Potential Alternatives to HFC-245fa in Organic Rankine Cycles. *Energy Procedia* **2017**, *142*, 1199–1205. https://doi.org/https://doi.org/10.1016/j.egypro.2017.12.381.

(3) Navarro-Esbrí, J.; Molés, F.; Peris, B.; Mota-Babiloni, A.; Kontomaris, K. Experimental Study of an Organic Rankine Cycle with HFO-1336mzz-Z as a Low Global Warming Potential Working Fluid for Micro-Scale Low Temperature Applications. *Energy* **2017**, *133*, 79–89. https://doi.org/https://doi.org/10.1016/j.energy.2017.05.092.

(4) Molés, F.; Navarro-Esbrí, J.; Peris, B.; Mota-Babiloni, A.; Barragán-Cervera, Á.; Kontomaris, K. (Kostas). Low GWP Alternatives to HFC-245fa in Organic Rankine Cycles for Low Temperature Heat Recovery: HCFO-1233zd-E and HFO-1336mzz-Z. *Appl. Therm. Eng.* **2014**, *71* (1), 204–212.

https://doi.org/https://doi.org/10.1016/j.applthermaleng.2014.06.055.

(5) Fouad, W. A.; Vega, L. F. Next Generation of Low Global Warming Potential Refrigerants: Thermodynamic Properties Molecular Modeling. *AIChE J.* **2018**, *64* (1), 250–262. https://doi.org/https://doi.org/10.1002/aic.15859.

(6) Rivela, C. B.; Tovar, C. M.; Teruel, M. A.; Barnes, I.; Wiesen, P.; Blanco, M. B. CFCs Replacements: Reactivity and Atmospheric Lifetimes of a Series of Hydrofluoroolefins towards OH Radicals and Cl Atoms. *Chem. Phys. Lett.* **2019**, *714*, 190–196. https://doi.org/https://doi.org/10.1016/j.cplett.2018.10.078.

(7) Rao, P. K.; Gejji, S. P. Atmospheric Degradation of HCFO-1233zd(E) Initiated by OH Radical, Cl Atom and O3 Molecule: Kinetics, Reaction Mechanisms and Implications. *J. Fluor. Chem.* **2018**, *211*, 180–193. https://doi.org/https://doi.org/10.1016/j.jfluchem.2018.05.001.

(8) Donahue, N. M.; Drozd, G. T.; Epstein, S. A.; Presto, A. A.; Kroll, J. H. Adventures in Ozoneland: Down the Rabbit-Hole. *Phys. Chem. Chem. Phys.* **2011**, *13* (23), 10848–10857. https://doi.org/10.1039/c0cp02564j.

(9) Osborn, D. L.; Taatjes, C. A. The Physical Chemistry of Criegee Intermediates in the Gas Phase. *Int. Rev. Phys. Chem.* **2015**, *34* (3), 309–360. https://doi.org/10.1080/0144235X.2015.1055676.

(10) Lester, M. I.; Klippenstein, S. J. Unimolecular Decay of Criegee Intermediates to OH Radical Products: Prompt and Thermal Decay Processes. *Acc. Chem. Res.* **2018**, *51* (4), 978–985. https://doi.org/10.1021/acs.accounts.8b00077.

(11) Chhantyal-Pun, R.; Khan, M. A. H.; Taatjes, C. A.; Percival, C. J.; Orr-Ewing, A. J.;

Shallcross, D. E. Criegee Intermediates: Production, Detection and Reactivity. *Int. Rev. Phys. Chem.* **2020**, *39* (3), 383–422. https://doi.org/10.1080/0144235X.2020.1792104.

(12) Wennberg, P. O.; Bates, K. H.; Crounse, J. D.; Dodson, L. G.; McVay, R. C.; Mertens, L. A.; Nguyen, T. B.; Praske, E.; Schwantes, R. H.; Smarte, M. D.; et al. Gas-Phase Reactions of Isoprene and Its Major Oxidation Products. *Chem. Rev.* **2018**, *118* (7), 3337–3390. https://doi.org/10.1021/acs.chemrev.7b00439.

(13) Nguyen, T. B.; Tyndall, G. S.; Crounse, J. D.; Teng, A. P.; Bates, K. H.; Schwantes, R. H.; Coggon, M. M.; Zhang, L.; Feiner, P.; Milller, D. O.; et al. Atmospheric Fates of Criegee Intermediates in the Ozonolysis of Isoprene. *Phys. Chem. Chem. Phys.* **2016**, *18* (15), 10241–10254. https://doi.org/10.1039/c6cp00053c.

(14) Womack, C. C.; Martin-Drumel, M. A.; Brown, G. G.; Field, R. W.; McCarthy, M. C. Observation of the Simplest Criegee Intermediate CH2OO in the Gas-Phase Ozonolysis of Ethylene. *Sci. Adv.* **2015**, *1* (2), 1–7. https://doi.org/10.1126/sciadv.1400105.

(15) Chen, T. Y.; Lee, Y. P. Dynamics of the Reaction CH2I + O2probed: Via Infrared Emission of CO, CO2, OH and H2CO. *Phys. Chem. Chem. Phys.* **2020**, *22* (31), 17540–17553. https://doi.org/10.1039/d0cp01940b.

(16) Li, J.; Guo, H. Full-Dimensional Potential Energy Surface and Ro-Vibrational Levels of Dioxirane. *J. Phys. Chem. A* **2016**, *120* (19), 2991–2998. https://doi.org/10.1021/acs.jpca.5b08491.

(17) Ting, A. W.-L. L.; Lin, J. J.-M. M. UV Spectrum of the Simplest Deuterated Criegee Intermediate CD2OO. *J. Chinese Chem. Soc.* **2017**, *64* (4), 360–368. https://doi.org/10.1002/jccs.201700049.

(18) Chang, Y. P.; Li, Y. L.; Liu, M. L.; Ou, T. C.; Lin, J. J. M. Absolute Infrared Absorption Cross Section of the Simplest Criegee Intermediate Near 1285.7 Cm-1. *J. Phys. Chem. A* **2018**, *122* (45), 8874–8881. https://doi.org/10.1021/acs.jpca.8b06759.

(19) Ting, W. L.; Chen, Y. H.; Chao, W.; Smith, M. C.; Lin, J. J. M. The UV Absorption Spectrum of the Simplest Criegee Intermediate CH 2OO. *Phys. Chem. Chem. Phys.* **2014**, *16* (22), 10438–10443. https://doi.org/10.1039/c4cp00877d.

(20) Smith, M. C.; Ting, W. L.; Chang, C. H.; Takahashi, K.; Boering, K. A.; Lin, J. J. M. UV Absorption Spectrum of the C2 Criegee Intermediate CH3CHOO. *J. Chem. Phys.* **2014**, *141* (7). https://doi.org/10.1063/1.4892582.

(21) Chang, Y.-P. P.; Chang, C.-H. H.; Takahashi, K.; Lin, J. J.-M. M. Absolute UV Absorption Cross Sections of Dimethyl Substituted Criegee Intermediate (CH3)2COO. *Chem. Phys. Lett.* **2016**, *653*, 155–160. https://doi.org/10.1016/j.cplett.2016.04.082.

(22) Sheps, L.; Scully, A. M.; Au, K. UV Absorption Probing of the Conformer-Dependent Reactivity of a Criegee Intermediate CH3CHOO. *Phys. Chem. Chem. Phys.* **2014**, *16* (48), 26701–26706.

(23) Sheps, L. Absolute Ultraviolet Absorption Spectrum of a Criegee Intermediate CH 2OO. *J. Phys. Chem. Lett.* **2013**, *4* (24), 4201–4205. https://doi.org/10.1021/jz402191w.

(24) Sršeň, Š.; Hollas, D.; Slavíček, P. UV Absorption of Criegee Intermediates: Quantitative Cross Sections from High-Level: Ab Initio Theory. *Phys. Chem. Chem. Phys.* **2018**, *20* (9), 6421–6430. https://doi.org/10.1039/c8cp00199e.

(25) Dawes, R.; Jiang, B.; Guo, H. UV Absorption Spectrum and Photodissociation Channels of the Simplest Criegee Intermediate (CH2OO). *J. Am. Chem. Soc.* **2015**, *137* (1), 50–53.

https://doi.org/10.1021/ja510736d.

(26) Aplincourt, P.; Henon, E.; Bohr, F.; Ruiz-López, M. F. Theoretical Study of Photochemical Processes Involving Singlet Excited States of Formaldehyde Carbonyl Oxide in the Atmosphere. *Chem. Phys.* **2002**, *285* (2–3), 221–231. https://doi.org/10.1016/S0301-0104(02)00804-2.

(27) Foreman, E. S.; Kapnas, K. M.; Jou, Y. T.; Kalinowski, J.; Feng, D.; Gerber, R. B.; Murray, C. High Resolution Absolute Absorption Cross Sections of the B1A′-X1A′ Transition of the CH2OO Biradical. *Phys. Chem. Chem. Phys.* **2015**, *17* (48), 32539–32546. https://doi.org/10.1039/c5cp04977f.

(28) Beames, J. M.; Liu, F.; Lu, L.; Lester, M. I. Ultraviolet Spectrum and Photochemistry of the Simplest Criegee Intermediate CH2OO. *J. Am. Chem. Soc.* **2012**, *134* (49), 20045–20048. https://doi.org/10.1021/ja310603j.

(29) Sheps, L.; Rotavera, B.; Eskola, A. J.; Osborn, D. L.; Taatjes, C. A.; Au, K.; Shallcross, D. E.; Khan, M. A. H.; Percival, C. J. The Reaction of Criegee Intermediate CH2OO with Water Dimer: Primary Products and Atmospheric Impact. *Phys. Chem. Chem. Phys.* **2017**, *19* (33), 21970–21979. https://doi.org/10.1039/c7cp03265j.

(30) Esposito, V. J.; Werba, O.; Bush, S. A.; Marchetti, B.; Karsili, T. N. V. Insights into the Ultrafast Dynamics of CH2OO and CH3CHOO Following Excitation to the Bright 1ππ* State: The Role of Singlet and Triplet States. *Photochem. Photobiol.* **2021**, *98*, 763–772. https://doi.org/10.1111/php.13560.

(31) McCoy, J. C.; Marchetti, B.; Thodika, M.; Karsili, T. N. V. A Simple and Efficient Method for Simulating the Electronic Absorption Spectra of Criegee Intermediates:

Benchmarking on CH2OO and CH3CHOO. *J. Phys. Chem. A* **2021**, *125* (19), 4089–4097. https://doi.org/10.1021/acs.jpca.1c01074.

(32) Esposito, V. J.; Liu, T.; Wang, G.; Caracciolo, A.; Vansco, M. F.; Marchetti, B.; Karsili, T. N. V.; Lester, M. I. Photodissociation Dynamics of CH2OO on Multiple Potential Energy Surfaces: Experiment and Theory. *J. Phys. Chem. A* **2021**, *125* (30), 6571–6579. https://doi.org/10.1021/acs.jpca.1c03643.

(33) McCoy, J. C.; Léger, S. J.; Frey, C. F.; Vansco, M. F.; Marchetti, B.; Karsili, T. N. V.; Marchetti, B.; Karsili, T. N. V. Modeling the Conformer-Dependent Electronic Absorption Spectra and Photolysis Rates of Methyl Vinyl Ketone Oxide and Methacrolein Oxide. *J. Phys. Chem. A* **2022**, *126* (4), 485–496. https://doi.org/10.1021/acs.jpca.1c08381.

(34) Wang, G.; Liu, T.; Zou, M.; Sojdak, C. A.; Kozlowski, M. C.; Karsili, T. N. V; Lester, M. I. Electronic Spectroscopy and Dissociation Dynamics of Vinyl-Substituted Criegee Intermediates: 2-Butenal Oxide and Comparison with Methyl Vinyl Ketone Oxide and Methacrolein Oxide Isomers. *J. Phys. Chem. A* **2022**. https://doi.org/10.1021/acs.jpca.2c08025.

(35) Antwi, E.; Bush, R.; Marchetti, B.; Karsili, T. A Direct Dynamics Study of the Exotic Photochemistry of the Simplest Criegee Intermediate, CH2OO. *Phys. Chem. Chem. Phys.* **2022**, *24*, 16724–16731.

(36) Antwi, E.; Packer, N. A.; Ratliff, J. M.; Marchetti, B.; Karsili, T. N. V. Insights into the Ultrafast Photodissociation Dynamics of Isoprene Derived Criegee Intermediates. *Photochem. Photobiol.* **2022**, DOI: https://doi.org/10.1111/php.13736.

(37) Antwi, E.; Ratliff, J. M.; Ashfold, M. N. R.; Karsili, T. N. V. Comparing the Excited State Dynamics of CH2OO, the Simplest Criegee Intermediate, Following Vertical versus Adiabatic Excitation. *J. Phys. Chem. A* **2022**, *126* (36), 6236–6243. https://doi.org/10.1021/acs.jpca.2c05118.

(38) Barbatti, M.; Granucci, G.; Persico, M.; Ruckenbauer, M.; Vazdar, M.; Eckert-Maksić, M.; Lischka, H. The On-the-Fly Surface-Hopping Program System Newton-X: Application to Ab Initio Simulation of the Nonadiabatic Photodynamics of Benchmark Systems. *J. Photochem. Photobiol. A Chem.* **2007**, *190* (2–3), 228–240. https://doi.org/10.1016/j.jphotochem.2006.12.008.

(39) Barbatti, M.; Ruckenbauer, M.; Plasser, F.; Pittner, J.; Granucci, G.; Persico, M.; Lischka, H. Newton-X: A Surface-Hopping Program for Nonadiabatic Molecular Dynamics. *Wiley Interdiscip. Rev. Comput. Mol. Sci.* **2013**, *4* (1), 26–33. https://doi.org/doi:10.1002/wcms.1158.

(40) Barber, V. P.; Pandit, S.; Green, A. M.; Trongsiriwat, N.; Walsh, P. J.; Klippenstein, S. J.; Lester, M. I. Four-Carbon Criegee Intermediate from Isoprene Ozonolysis: Methyl Vinyl Ketone Oxide Synthesis, Infrared Spectrum, and OH Production. *J. Am. Chem. Soc.* **2018**, *140* (34), 10866–10880. https://doi.org/10.1021/jacs.8b06010.

(41) Wang, G.; Liu, T.; Caracciolo, A.; Vansco, M. F.; Trongsiriwat, N.; Walsh, P. J.; Marchetti, B.; Karsili, T. N. V; Lester, M. I. Photodissociation Dynamics of Methyl Vinyl Ketone Oxide: A Four-Carbon Unsaturated Criegee Intermediate from Isoprene Ozonolysis. *J. Chem. Phys.* **2021**, *155* (17), 174305. https://doi.org/10.1063/5.0068664.

(42) Wang, G.; Liu, T.; Zou, M.; Sojdak, C. A.; Kozlowski, M. C.; Karsili, T. N. V; Lester, M.

I. Electronic Spectroscopy and Dissociation Dynamics of Vinyl-Substituted Criegee Intermediates: 2-Butenal Oxide and Comparison with Methyl Vinyl Ketone Oxide and Methacrolein Oxide Isomers. *J. Phys. Chem. A* **2023**, *127* (1), 203–215. https://doi.org/10.1021/acs.jpca.2c08025.

(43) McGillen, M. R.; Curchod, B. F. E.; Chhantyal-Pun, R.; Beames, J. M.; Watson, N.; Khan, M. A. H.; McMahon, L.; Shallcross, D. E.; Orr-Ewing, A. J. Criegee Intermediate-Alcohol Reactions, A Potential Source of Functionalized Hydroperoxides in the Atmosphere. *ACS Earth Sp. Chem.* **2017**, *1* (10), 664–672. https://doi.org/10.1021/acsearthspacechem.7b00108.

(44) Yu, X.; Hou, H.; Wang, B. Atmospheric Chemistry of Perfluoro-3-Methyl-2-Butanone [CF3C(O)CF(CF3)2]: Photodissociation and Reaction with OH Radicals. *J. Phys. Chem. A* **2018**, *122* (45), 8840–8848. https://doi.org/10.1021/acs.jpca.8b09111.

(45) Francés-Monerris, A.; Carmona-García, J.; Acuña, A. U.; Dávalos, J. Z.; Cuevas, C. A.; Kinnison, D. E.; Francisco, J. S.; Saiz-Lopez, A.; Roca-Sanjuán, D. Photodissociation Mechanisms of Major Mercury(II) Species in the Atmospheric Chemical Cycle of Mercury. *Angew. Chemie - Int. Ed.* **2020**, *59* (19), 7605–7610. https://doi.org/10.1002/anie.201915656.

(46) Prlj, A.; Ibele, L. M.; Marsili, E.; Curchod, B. F. E. On the Theoretical Determination of Photolysis Properties for Atmospheric Volatile Organic Compounds. *J. Phys. Chem. Lett.* **2020**, *11* (14), 5418–5425. https://doi.org/10.1021/acs.jpclett.0c01439.

(47) Röder, A.; De Oliveira, N.; Grollau, F.; Mestdagh, J. M.; Gaveau, M. A.; Briant, M. Vacuum-Ultraviolet Absorption Spectrum of 3-Methoxyacrylonitrile. *J. Phys. Chem. A*

2020, *124* (45), 9470–9477. https://doi.org/10.1021/acs.jpca.0c08974.

(48) Rodrigues, G. P.; Ventura, E.; Andrade Do Monte, S.; Barbatti, M. UV-Photoexcitation and Ultrafast Dynamics of HCFC-132b (CF2ClCH2Cl). *J. Comput. Chem.* **2016**, *37* (7), 675–683. https://doi.org/10.1002/jcc.24260.

(49) Saiz-Lopez, A.; Sitkiewicz, S. P.; Roca-Sanjuán, D.; Oliva-Enrich, J. M.; Dávalos, J. Z.; Notario, R.; Jiskra, M.; Xu, Y.; Wang, F.; Thackray, C. P.; et al. Photoreduction of Gaseous Oxidized Mercury Changes Global Atmospheric Mercury Speciation, Transport and Deposition. *Nat. Commun.* **2018**, *9* (1), 4796. https://doi.org/10.1038/s41467-018-07075-3.

(50) Butcher, J. C. A Modified Multistep Method for the Numerical Integration of Ordinary Differential Equations. *J. ACM* **1965**, *12* (1), 124–135. https://doi.org/10.1145/321250.321261.

(51) Park, J. W.; Shiozaki, T. Analytical Derivative Coupling for Multistate CASPT2 Theory. *J. Chem. Theory Comput.* **2017**, *13* (6), 2561–2570. https://doi.org/10.1021/acs.jctc.7b00018.

(52) Shiozaki, T. BAGEL: Brilliantly Advanced General Electronic-Structure Library. *Wiley Interdiscip. Rev. Comput. Mol. Sci.* **2018**, *8* (1), e1331. https://doi.org/10.1002/wcms.1331.

(53) Kraka, E.; Konkoli, Z.; Cremer, D.; Fowler, J.; Schaefer, H. F. Difluorodioxirane: An Unusual Cyclic Peroxide. *J. Am. Chem. Soc.* **1996**, *118* (43), 10595–10608. https://doi.org/10.1021/ja961983w.

(54) Antwi, E.; Bush, R.; Marchetti, B.; Karsili, T. A Direct Dynamics Study of the Exotic

Photochemistry of the Simplest Criegee Intermediate, CH2OO. *Phys. Chem. Chem. Phys.* **2022**, *24*, 16724–16731. https://doi.org/10.1039/d2cp01860h.

TOC Graphic

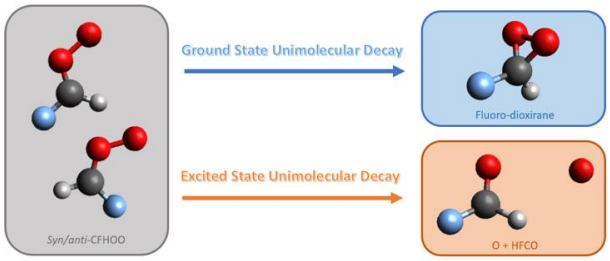
Ground State Unimolecular Decay
Excited State Unimolecular Decay
Syn/anti-CFHOO
Fluoro-dioxirane
O + HFCO